Research Article

Xueming Yang*, Jixiang Cui, Ke Xue, Yao Fu, Hanling Li, and Hong Yang

Thermal conductivity and thermoelectric properties in 3D macroscopic pure carbon nanotube materials

https://doi.org/10.1515/ntrev-2021-0013
received February 22, 2021; accepted March 16, 2021

Abstract: Sintered carbon nanotube (CNT) blocks and porous CNT sponges were prepared, and their thermoelectric properties were measured. The maximum dimensionless thermoelectric figure-of-merit, ZT, at room temperature of the sintered single-walled carbon nanotube (SWCNT) block is 9.34×10^{-5}, which is twice higher than that of the sintered multi-walled carbon nanotube (MWCNT) block in this work and also higher than that of other sintered MWCNT blocks reported previously. In addition, the porous MWCNT sponge showed an ultra-low thermal conductivity of 0.021 W/(m K) and significantly enhanced ZT value of 5.72×10^{-4} at room temperature and 1 atm. This ZT value is higher than that of other 3D macroscopic pure CNT materials reported. The pronounced enhancement of the ZT in the porous MWCNT sponge is attributed to the ultra-low density, ultra-high porosity, and interconnected structure of the material, which lead to a fairly low thermal conductivity and better Seebeck coefficient. The finding of this work provides an understanding for exploring potential enhancement mechanisms and improving the thermoelectric properties of CNT-based thermoelectric composites.

Keywords: thermal conductivity, carbon nanotubes, thermoelectric properties, Seebeck coefficient

*** Corresponding author: Xueming Yang,** Department of Power Engineering, North China Electric Power University, Baoding 071003, China, e-mail: xuemingyang@ncepu.edu.cn
Jixiang Cui, Ke Xue: Department of Power Engineering, North China Electric Power University, Baoding 071003, China
Yao Fu: Department of Aerospace Engineering and Engineering Mechanics, University of Cincinnati, Cincinnati, OH 45221-0070, United States of America
Hanling Li: Department of Engineering Mechanics, Tsinghua University, Beijing 100084, China
Hong Yang: Department of Electronic Engineering, North China Electric Power University, Baoding 071003, China

1 Introduction

Thermoelectric materials have attracted considerable attention because of their unique ability of direct conversion between thermal and electrical energy [1–4]. Performance of thermoelectric materials is given by the dimensionless figure-of-merit, $ZT = S^2\sigma T/k$, where T, S, σ, and k are the temperature, Seebeck coefficient, electrical conductivity, and thermal conductivity, respectively [5,6]. The carbon nanotubes (CNTs) have unique electrical conductivity, and their thermal conductivity can be tuned by varying the morphology and structure, thus have been considered as promising thermoelectric materials [7–9]. Prasher *et al.* [9] first measured the thermal conductivity and thermoelectric power of single-walled carbon nanotube (SWCNT) packed bed at a pressure of 20–90 psi. The ZT was estimated theoretically up to 0.0047. However, CNT packed bed is not suitable to be directly used as the thermoelectric materials because of its unassembled structure.

The dense CNT films, ropes, or fibers in microscale and nanoscale were found to have high ZT. These CNT materials have relatively high mass density, thus making a good power factor. Hone *et al.* [10] prepared aligned SWCNT films (thickness of 1.3 and 5 μm; mass density of 1.33 g/cm^3) and nanotube ropes by filtration/deposition from suspension in strong magnetic fields, and the measured ZT reached 1×10^{-4} at room temperature. Zhou *et al.* [11] prepared a SWCNT interconnected film with a thickness of 600 nm. The grown SWCNT film exhibited an excellent power factor (2,482 μW/m K^2) at room temperature, and the ZT of the SWCNT fiber obtained by twisting these films reached 0.014.

As for CNT composite materials, Toshima *et al.* [12] prepared a flexible composite thermoelectric film based on CNT by complexing nickel-coordinating polymers of vinyl tetrathiol and polyvinyl chloride film. A ternary composite film with a conductivity of 630 S/cm and a thermal conductivity of only 0.07 W/(m K) was obtained.

The *ZT* of the composite film has reached 0.3 and is considered as one of the best performing CNT-based flexible films. Tan *et al.* [13] developed rGO/SWCNT hybrid aerogels with extreme low density 10 mg/cm^3 by constructing 3D double-interconnected network porous microstructures. The hybrid aerogel reveals very low thermal conductivity and a high figure-of-merit of 8.03×10^{-3}. These CNT composite materials generally have extreme low density and high porosity, thus leading to a fairly low thermal conductivity. However, most of the experimental studies on the CNT composite based nanofilm were conducted with only the power factor focused on, primarily because of the difficulty to accurately measure the thermal conductivity of thin film samples [14–16].

So far, the reported *ZT* of 3D macroscopic pure CNT materials is fairly low. Jin *et al.* [17] measured the thermoelectric properties of macroscopic bundles of long multi-walled carbon nanotube (MWCNT) annealed in argon (Ar) at 2,800°C, the *ZT* of the MWCNT bulk reached 5.4×10^{-5} at room temperature. Qin *et al.* [18] prepared bulk multi-walled CNT by spark plasma sintering (SPS). The thermoelectric properties of the bulk material were measured in the directions perpendicular and parallel to the pressure direction. Both the thermal conductivity and electrical conductivity show apparent anisotropy, but the thermoelectric power has close values in the two different directions and the *ZT* of SWCNT bulk reached 4.3×10^{-5} at room temperature. Yang *et al.* [19] prepared aligned MWCNT bulk samples by SPS method with the *ZT* value of 2.58×10^{-6} at room temperature. They also prepared and measured the SPS sintered multi-walled CNT buckypaper, and interestingly, the *ZT* at room temperature decreased from 4.07×10^{-5} to 1.29×10^{-5} when SPS temperatures increased from 900 to 1,500°C. Compared to the above 3D macroscopic pure CNT materials with high mass density, porous CNT sponges can exhibit better *ZT*. Chen *et al.* [20] prepared the MWCNT sponges by chemical vapor deposition (CVD) and found their *ZT* reached 3.85×10^{-4} in standard atmosphere at room temperature.

In this study, we focused on the thermal conductivity and thermoelectric properties of 3D macroscopic pure CNT materials, including the SPS sintered SWCNT and MWCNT bulk materials and MWCNT sponge. The objective of our work is to provide a clear understanding of the thermal conductivity and thermoelectric properties for pure CNT bulk materials via our comprehensive experimental research. This study could provide help in exploring potential enhancement mechanisms and improving the thermoelectric properties of CNT-based thermoelectric composites.

2 Experiment

The SWCNT and MWCNT powders for the preparation of the sintered CNT blocks are purchased from Chengdu Organic Chemicals Co. Ltd (Chinese Academy of Sciences). The purity of SWCNT is greater than 95%, and the SWCNT has an average outer diameter of 1–2 nm and an average length of 1–3 μm. The MWCNT has an average outer diameter of 4–6 nm, an average length of 0.5–2 μm, and purity greater than 98%. It should be noted that the length of both the SWCNT and MWCNT of the purchased samples is much shorter than those in the literature (*e.g.*, an average length of 5–15 μm in ref. [9]), since we attempted to investigate whether shorter length CNT can enhance the *ZT* by the reduction in thermal conductivity.

The thermal conductivity of the two CNT stacked states was measured using a transient hot-wire method (TC3000E, XIA TECH, CHN). The resistivity, Seebeck coefficient, and thermal conductivity of the SPS sintered CNT bulk samples were measured using a PPMS (Quantum Design, PPMS-9) at a temperature of 300 K. The conductivity and Seebeck coefficient of CNT sponge were measured using a SBA 458 Nemesis (Netzsch). The thermal diffusivity was measured using a laser flash method (Netzsch LFA 467) after spray coated with graphite to enhance emissivity. The heat capacities were measured using a differential scanning calorimeter (TA Q5000). The measurements were performed in Ar atmosphere under normal pressure around 1 atm. The thermal conductivity k of the samples was calculated using $k = D\rho C_p$, where D is the thermal diffusivity, ρ is the mass density, and C_p is the heat capacity. Because of the different instruments used in the measurements, resistivity and conductivity directly measured were given in this paper.

3 Results and discussions

3.1 Preparation of SPS sintered SWCNT and MWCNT blocks

The CNT powder was stacked in a graphite mold (pore size ~20 mm). Then, the powder was sintered using an SPS apparatus (SPS-20T-10, Shanghai Chen Hua Technology Co., China). A constant pressure of 40 MPa was maintained in all SPS experiments while changing the applied current density to achieve different SPS temperatures (T_{SPS}). We sintered the CNTs at 1,200, 1,400, 1,600, 1,800, and 2,000°C in vacuum for 5 min. The obtained typical sintered CNT blocks are shown in Figure 1a and b.

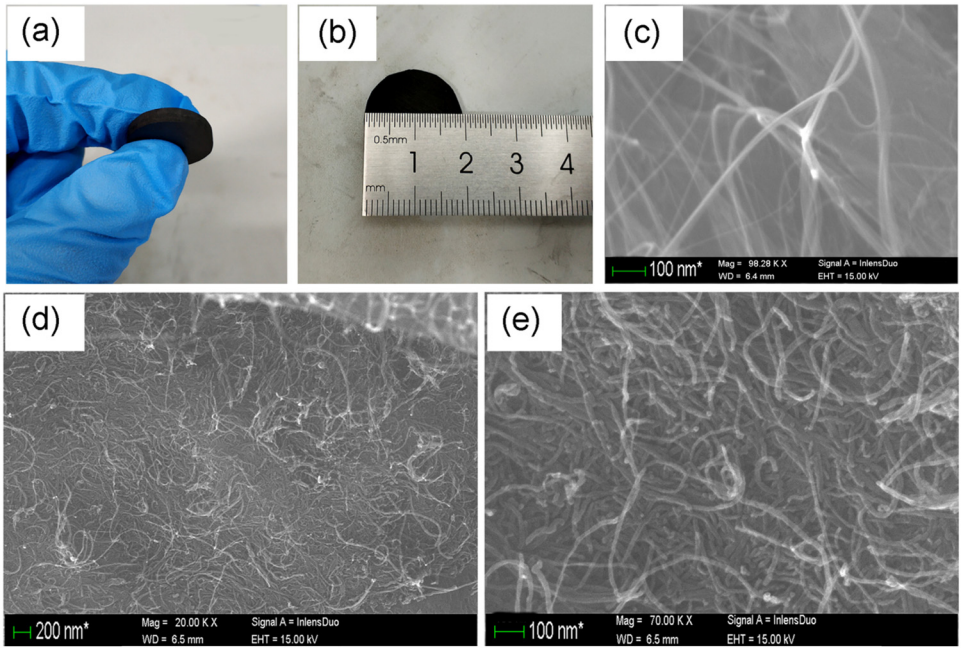

Figure 1: (a) and (b) SPS sintered SWCNT blocks; (c) scanning electron microscopy (SEM) image of the polished surface; (d) and (e) low-resolution and high-resolution SEM image showing fracture surfaces of the bulk SWCNT materials.

3.2 Morphological characterization of SPS sintered SWCNT and MWCNT blocks

The microscopic morphology of the CNT macroscopic material was characterized by scanning electron microscopy (Zeiss, Merlin compact). Here we take the bulk SWCNT materials sintered at 2,000°C as an example. Figure 1c shows the SEM image of the polished surface of the sintered bulk SWCNT sample. It can be observed that some covalently bonded junctions are formed because of the local high temperature to join SWCNT together [21]. Similarly, local welding of SWCNT (inter-tube bonds) also can be observed on the fracture surfaces of the bulk SWCNT materials, as shown in Figure 1d and e.

3.3 Preparation of CNT sponge

A MWCNT sponge using a CVD method by Gui *et al.* was prepared [22,23]. The main ingredient of the sponge is MWCNT, with purity of over 90%, which is consistent with previous reports. An MWCNT sponge with a density of 5.3 mg/cm^3 (Figure 2a and b) was prepared. The as-grown MWCNT sponge is shown as a black carpet with a thickness of 2.37 mm (Figure 2b).

3.4 Structural and morphological characterizations of CNT sponge

The SEM image of the sponge is shown in Figure 2c and d shows more detailed microstructure of the sample. It can be observed that the CNT sponge is a 3D porous network structure in which CNTs are entangled with each other and self-assembled. We also observed that the CNTs had a very high void ratio. The CNT sponge has the characteristics of isotropy. SEM at higher magnifications shows that CNTs have uniform diameter with scarce iron catalyst remained. The average diameter of CNTs is around 30 nm.

3.5 Measurement results and discussion

Figure 3a demonstrates the change in measured thermal conductivity k with mass density of SWCNT and MWCNT packed bed that can be typically considered as unconnected randomly oriented CNTs network. It can be seen that k for both the SWCNT and MWCNT packed bed increases linearly with the increase in the mass density, *e.g.*, $k \propto \rho$, and k of SWCNT increases more significantly with the mass density than those of the MWCNT packed bed. When ρ_{SWCNTs} increased from 0.097 to 0.217 g/cm^3,

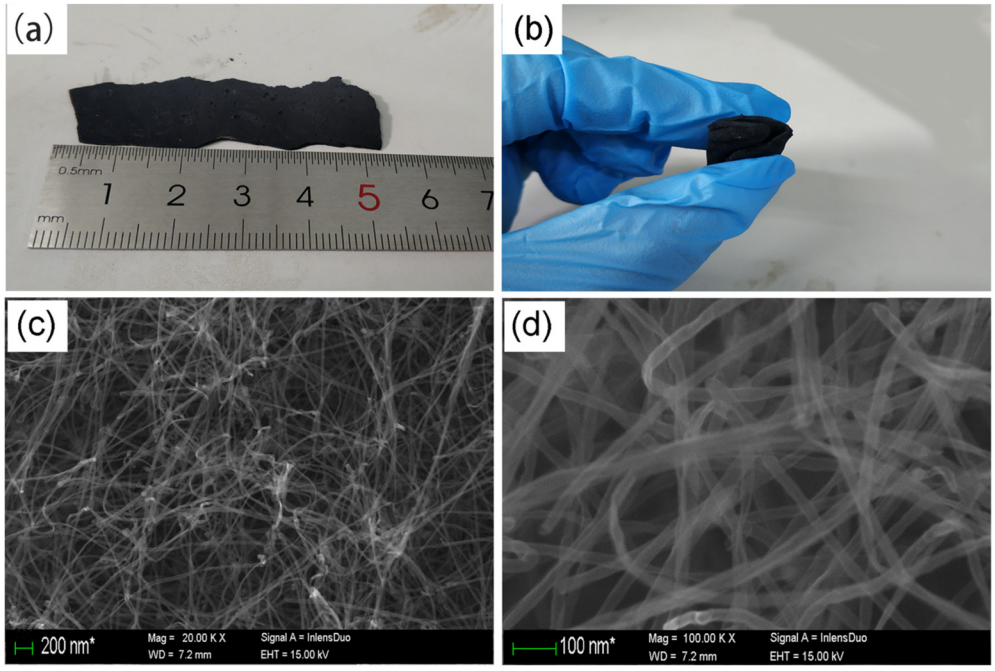

Figure 2: (a) and (b) Prepared MWCNT sponge; (c) and (d) low-resolution and high-resolution SEM image showing the random CNT network of sponges.

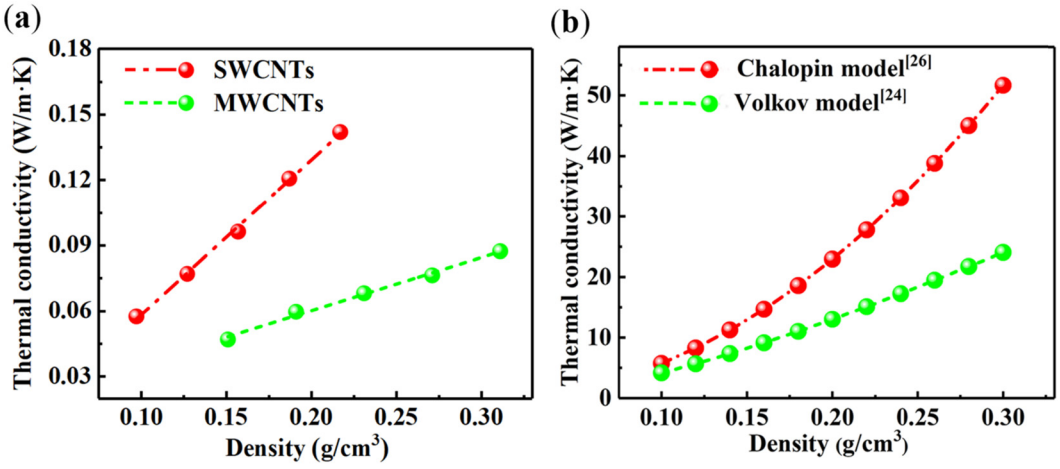

Figure 3: Thermal conductivity of the SWCNT and MWCNT packed bed as a function of density: (a) experimental results; (b) calculation results by Chalopin's model [24] and Volkov's model [26].

k_{SWCNTs} was enhanced from 0.057 to 0.142 W/(m K). As ρ_{MWCNTs} increases from 0.151 to 0.311 g/cm^3, k_{MWCNTs} was enhanced from 0.047 to 0.087 W/(m K). Here k_{SWCNTs} was obviously higher than k_{MWCNTs} at the same mass density, mainly because the average length of the SWCNT (1–3 μm) is larger than that of the MWCNT (0.5–2 μm). The thermal conductivity obtained for SWCNT and MWCNT packed bed is also less than the results obtained by the Prasher *et al.* [9], because of the shorter length of the tubes in this work. To the best of our knowledge, there exist no experimental studies on the mass density dependence of thermal conductivity of CNT packed bed. We thus resort to the theoretical studies of Volkov and Zhigilei [24,25] and Chalopin *et al.* [26] on the thermal conductivity of the CNT network as a function of mass density and tube length. The Chalopin's model is based on the assumption that the axial thermal conductivity of individual CNT is infinite, whereas Volkov's model [24] considered the thermal

conductivity of individual CNT as a finite value. The model predictions are shown in Figure 3b. It can be observed that the results by Volkov's model generally follow a linear relation $k \propto \rho$ and those of Chalopin's model follow a parabolic relation $k \propto \rho^2$ when the length of the SWCNT is set as 1.5 µm. Therefore, a better agreement can be found between our experimental results and Volkov's model. However, it can also be observed that the predictions by both Volkov's model and Chalopin's model have much larger values than those of the experimental results. As mentioned by Volkov and Zhigilei [24,25], the theoretical predictions can often be one or two orders different from the experimental results. These theoretical models can thus provide a semi-quantitative analysis of the effect of the mass density and length tube on thermal conductivity of SWCNT networks consisted of pristine tubes.

Figure 4(a–d) shows the thermal resistivity, Seebeck coefficient, resistivity, and calculated *ZT* values of the sintered CNT blocks at different SPS temperature (T_{SPS}). With the increase in T_{SPS}, the thermal conductivity at room temperature for SWCNT samples increases from 0.89 to 1.34 W/(m K) and that of the MWCNT samples increases from 0.59 to 1.07 W/(m K). Such increase in thermal conductivity is supposed to result from the increase in the mass density. Moreover, with the increase in the T_{SPS}, more covalently bonded junctions between the tubes are formed via heat welding, and the overall tube–tube thermal resistance is decreased [27,28]. This could also explain that the thermal conductivity of the SPS sintered CNT blocks is significantly enhanced compared with the corresponding CNT packed bed. It should be noted that the thermal conductivities of the SPS sintered CNT blocks in this work are much lower than those in refs. [17–19,29,30] because our target is to improve the *ZT* value, and thus shorter CNTs were used.

The Seebeck coefficient *S* of the SWCNT samples is higher than that of the MWCNT samples at different T_{SPS}, which is consistent with the results of the annealed dense and thick SWCNT films by Hone *et al.* [10] and the SPS sintered bulk MWCNT by Qin *et al.* [18]. The measured resistivity of both SWCNT and MWCNT samples shows a

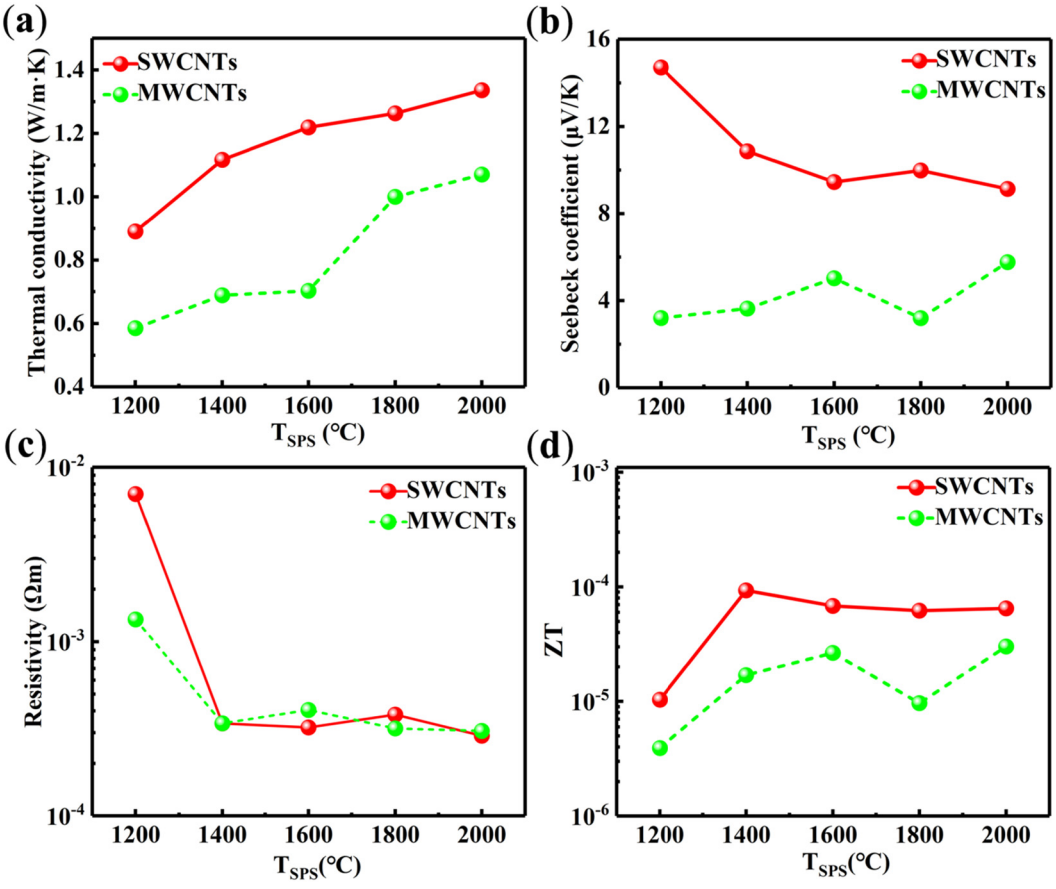

Figure 4: SPS temperature dependence of (a) thermal conductivity; (b) Seebeck coefficient; (c) resistivity; (d) *ZT*; for single-wall and multi-walled CNT blocks.

significant drop at T_{SPS} of 1,400°C, followed by a plateau when T_{SPS} was above 1,400°C. The lowest resistivity of sintered SWCNT samples is 2.89×10^{-4} Ωm which is two orders higher than the resistivity value of about 1×10^{-6} Ωm for the aligned SWCNT [10], attributed to the characteristic of the 3D random distribution of the sintered SWCNT samples. Meanwhile, the lowest resistivity of MWCNT samples is 3.08×10^{-4} Ωm, which is about two times higher than that of the previously reported sintered MWCNT samples [19], possibly attributed to the shorter length of MWCNT. The *ZT* value of MWCNT block is about 3.03×10^{-5} which is equivalent to the *ZT* value of previously reported MWCNT sintered block [19]. However, the sintered SWCNT block has a maximum *ZT* value of 9.34×10^{-5}, which is much higher than the MWCNT sintered block in this work or that reported before. Overall, it is shown that SWCNT has better performance compared to MWCNT.

Figure 5(a–d) shows the thermal conductivity, Seebeck coefficient, electrical conductivity, and calculated *ZT* of the CNT sponge as a function of temperature, respectively, and compared with the thermoelectric properties of MWCNT sponges reported by Chen *et al.* [20]. The ultra-high porosity of the CNT sponge is responsible for the low thermal conductivity and good thermal insulation property. As shown in Figure 5a, the MWCNT sponges in this work exhibit an ultra-low thermal conductivity value of 0.021 W/(m K) which is 67% lower than that of the MWCNT sponges by Chen *et al.* [20] measured at a temperature of 300 K and 1 atm. The Seebeck coefficient is positive and increases as temperature increases, which is in agreement with those of CNT samples in other literature [19,20]. The positive Seebeck coefficient can be explained by hole-type majority carriers and the hole doping effect [20,31,32]. Figure 5(c) shows the comparison of the electrical conductivity of the sponges. It can be seen that the conductivity of our sponge is about 30% less than that by Chen *et al.* [20] because the mass density of our sponge is only about half of the latter. As shown in Figure 5(d), the *ZT* of the sponge shows a significant enhancement with a value of 5.72×10^{-4} at room temperature and 1 atm. In fact, the power factor, $S^2\sigma$, of the MWCNT sponge in this work and that by Chen *et al.* [20] is comparable. This can be understood by the low density of MWCNT sponges which is about half

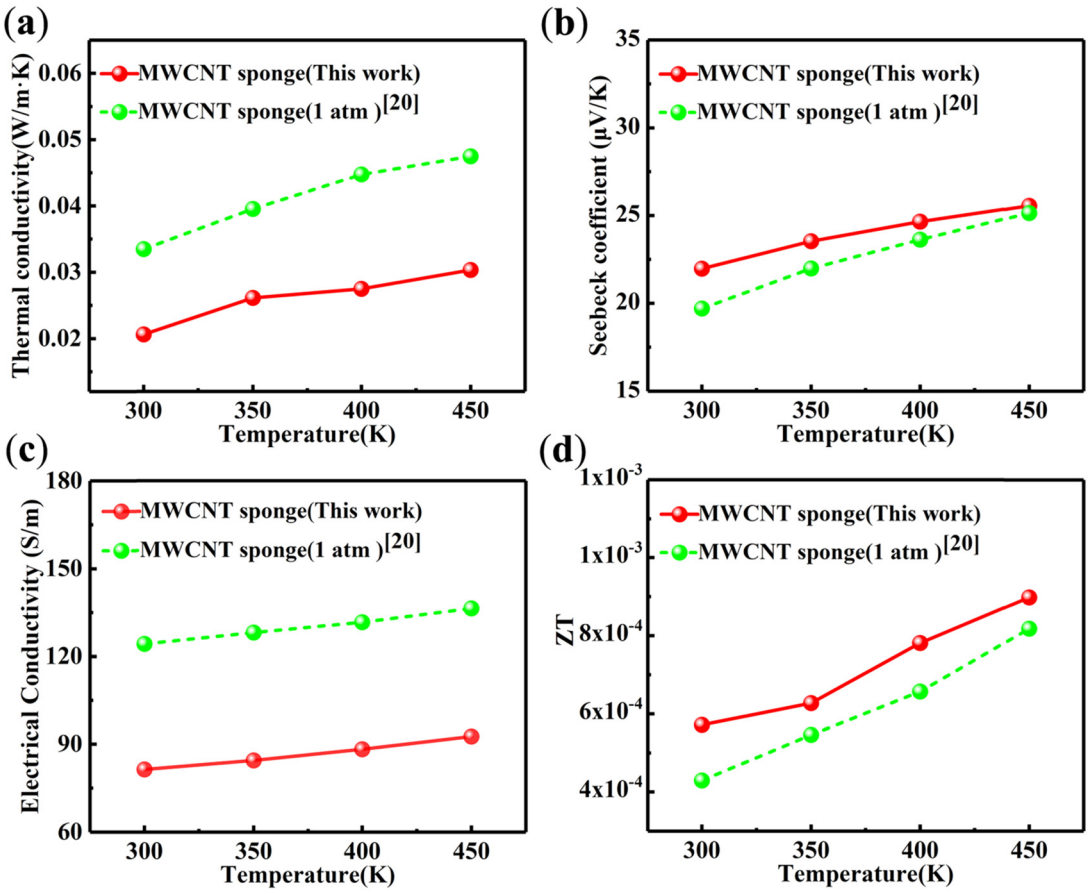

Figure 5: Temperature dependence of (a) thermal conductivity; (b) Seebeck coefficient; (c) conductivity; (d) *ZT*; of the MWCNT sponges.

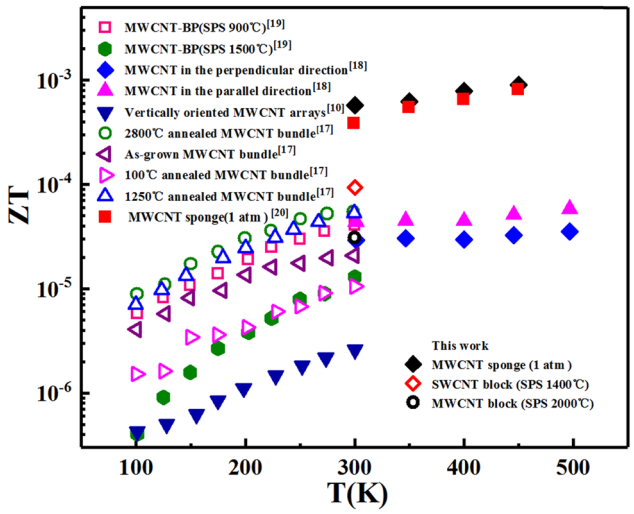

Figure 6: Comparison of temperature dependence of *ZT* values for samples prepared in this paper and other macroscopic pure CNTs materials.

of that by Chen *et al.* [20], which leads to a decrease in thermal conductivity which decreases with the mass density [24–26] and thus enhanced *ZT* values.

The comparison of *ZT* values between the results of this work and other 3D macroscopic pure CNT materials [10,17–20] is shown in Figure 6. The maximum *ZT* value of the MWCNT sintered block in this work is about 3.03×10^{-5}, equivalent to the previously reported the MWCNT sintered block. The *ZT* value of the SWCNT sintered block is about three times as high as that of the MWCNT sintered block, higher than that of other CNT block materials. The *ZT* value of the MWCNT sponge prepared in this work reaches a maximum of 5.72×10^{-4} at room temperature and 1 atm, superior to other 3D macroscopic pure CNT materials and improved by an order of magnitude. However, it is worth mentioning that although the CNT sponge prepared in this paper has ultra-low thermal conductivity, the Seebeck coefficient and the conductivity are not superior.

The sintered CNT bulk materials and CNT sponge represented two different routes in enhancing the thermoelectric figure of merit for 3D macroscopic pure CNT materials. The former attempts to improve *ZT* by increasing σ, while the latter by decreasing k. The mass density of MWCNT sponge was decreased by 322 times as compared with the sintered MWCNT blocks at T_{SPS} = 2,000°C. Although this resulted in a 38.9 times reduction in electrical conductivity for the MWCNT sponge, a 50.9 times reduction in thermal conductivity and a 2.81 times increase in Seebeck coefficient are obtained, which leads to a much higher *ZT* than that of sintered MWCNT blocks. This suggested that CNT sponge with ultralow thermal conductivity and good Seebeck coefficient can be a promising candidate for CNT-based thermoelectric composites.

4 Conclusion

In summary, the thermal conductivity and thermoelectric properties of sintered CNTs and porous CNT sponges were investigated. It is found that the maximum *ZT* at room temperature of the SPS sintered SWCNT blocks is 9.33×10^{-5}, twice higher than that of the sintered MWCNT blocks in this work and also higher than that of other sintered MWCNT blocks reported previously. Therefore, SWCNT block is a better alternative than its MWCNT counterpart. Moreover, MWCNT sponge with super low mass density is prepared and measured. It was found that MWCNT sponges showed an ultra-low thermal conductivity of 0.021 W/(m K) and significantly enhanced *ZT* value of 5.72×10^{-4} at room temperature and 1 atm, which is higher than other reported 3D macroscopic pure CNT materials. The significant enhancement in *ZT* of the porous MWCNT sponges is attributed to the ultra-low density, ultra-high porosity, and interconnected structure of material, which lead to a fairly low thermal conductivity and better Seebeck coefficient. This work presents two different routes in enhancing the thermoelectric properties of CNT-based materials, and the finding provides a crucial understanding in exploring potential enhancement mechanisms.

Another contribution of this study is to bring readers a clear understanding of the thermal conductivity and thermoelectric properties for 3D macroscopic pure CNT materials via our comprehensive experimental research. Although many scholars have expected that the pure CNT bulk materials can be as promising thermoelectric materials, our work shows clearly that the *ZT* values achieved in 3D macroscopic pure CNT materials are still poor (on the level of 10^{-4} even it is significant enhanced) compared to the recent progress of thermoelectric field [33–49].

Acknowledgments: The authors thank Prof. Anyuan Cao and Dr. Yizeng Wu from Peking University for their kind support and assistance in the preparation of the samples of MWCNT Sponges.

Funding information: This research was supported by the National Natural Science Foundation of China (Grant Nos. 52076080 and 51576066) and the Natural Science

Foundation of Hebei Province of China (Grant No. E2019502138).

Author contributions: Xueming Yang: conceptualization, methodology, validation, formal analysis, investigation, project administration, writing – original draft. Jixiang Cui: writing – review & editing, validation, data curation. Ke Xue: investigation, validation, writing – original draft. Yao Fu: writing – review and editing. Hanling Li: formal analysis, validation. Hong Yang: validation. All authors have accepted responsibility for the entire content of this manuscript and approved its submission.

Conflict of interest: The authors state no conflict of interest.

References

[1] Chandel VS, Wang G, Talha M. Advances in modelling and analysis of nano structures: a review. Nanotechnol Rev. 2020;9(1):230–58.
[2] Lu W, Li S, Xu R, Zhang J, Li D, Feng Z, et al. Boosting thermoelectric performance of SnSe via tailoring band structure, suppressing bipolar thermal conductivity, and introducing large mass fluctuation. ACS Appl Mater Interfaces. 2019;11(48):45133–41.
[3] Alsalama MM, Hamoudi H, Abdala A, Ghouri ZK, Youssef KM. Enhancement of thermoelectric properties of layered chalcogenide materials. Rev Adv Mater Sci. 2020;59(1):371.
[4] Jung DH, Sharma A, Mayer M, Jung JP. A review on recent advances in transient liquid phase (TLP) bonding for thermoelectric power module. Rev Adv Mater Sci. 2018;53(2):147–60.
[5] Wang G, Chen Q, Gao M, Yang B, Hui D. Generalized locally-exact homogenization theory for evaluation of electric conductivity and resistance of multiphase materials. Nanotechnol Rev. 2020;9(1):1–16.
[6] Ma W, Liu Y, Yan S, Miao T, Shi S, Yang M, et al. Systematic characterization of transport and thermoelectric properties of a macroscopic graphene fiber. Nano Res. 2016;9(11):3536–46.
[7] Behdinan K, Moradi-Dastjerdi R, Safaei B, Qin Z, Chu F, Hui D. Graphene and CNT impact on heat transfer response of nanocomposite cylinders. Nanotechnol Rev. 2020;9(1):41–52.
[8] Dassan EGB, Anjang A, Rahman A, Shukur M, Abidin Z, Akil HM. Carbon nanotube-reinforced polymer composite for electromagnetic interference application: a review. Nanotechnol Rev. 2020;9(1):768–88.
[9] Prasher RS, Hu X, Chalopin Y, Mingo N, Lofgreen K, Volz S, et al. Turning carbon nanotubes from exceptional heat conductors into insulators. Phys Rev Lett. 2009;102(10):1–4.
[10] Hone J, Llaguno MC, Nemes NM, Johnson AT, Fischer JE, Walters DA, et al. Electrical and thermal transport properties of magnetically aligned single wall carbon nanotube films. Appl Phys Lett. 2000;77(5):666–8.
[11] Zhou W, Fan Q, Zhang Q, Li K, Cai L, Gu X, et al. Ultrahigh-power-factor carbon nanotubes and an ingenious strategy for thermoelectric performance evaluation. Small. 2016;12(25):3407–14.
[12] Toshima N, Oshima K, Anno H, Nishinaka T, Ichikawa S, Iwata A, et al. Novel hybrid organic thermoelectric materials: three-component hybrid films consisting of a nanoparticle polymer complex, carbon nanotubes, and vinyl polymer. Adv Mater. 2015;27(13):2246–51.
[13] Tan D, Zhao J, Gao C, Wang H, Chen G, Shi D. Carbon nanoparticle hybrid aerogels: 3D double-interconnected network porous microstructure, thermoelectric, and solvent-removal functions. ACS Appl Mater Interfaces. 2017;9(26):21820–8.
[14] Lee W, Hong CT, Kwon OH, Yoo Y, Kang YH, Lee JY, et al. Enhanced thermoelectric performance of bar-coated SWCNT/P3HT thin films. ACS Appl Mater Interfaces. 2015;7(12):6550–6.
[15] Li D, Luo C, Chen Y, Feng D, Gong Y, Pan C, et al. High performance polymer thermoelectric composite achieved by carbon-coated carbon nanotubes network. ACS Appl Energy Mater. 2019;2(4):2427–34.
[16] Feng N, Gao C, Guo C, Chen G. Copper-phenylacetylide nanobelt/single-walled carbon nanotube composites: mechanochromic luminescence phenomenon and thermoelectric performance. ACS Appl Mater Interfaces. 2018;10(6):5603–8.
[17] Jin R, Zhou Z, Mandrus D, Ivanov IN, Eres G, Howe JY, et al. The effect of annealing on the electrical and thermal transport properties of macroscopic bundles of long multi-wall carbon nanotubes. Phys B Condens Matter. 2007;388(1–2):326–30.
[18] Qin C, Shi X, Bai S, Chen L, Wang L. High temperature electrical and thermal properties of the bulk carbon nanotube prepared by SPS. Mater Sci Eng A. 2006;420(1–2):208–11.
[19] Yang K, He J, Puneet P, Su Z, Skove MJ, Gaillard J, et al. Tuning electrical and thermal connectivity in multiwalled carbon nanotube buckypaper. J Phys Condens Matter. 2010;22(33):334215.
[20] Chen J, Gui X, Wang Z, Li Z, Xiang R, Wang K, et al. Superlow thermal conductivity 3D carbon nanotube network for thermoelectric applications. ACS Appl Mater Interfaces. 2012;4(1):81–6.
[21] Zhang Z, Qi L, Shen X, Wang F, Lee SK. Microstructure and mechanical properties of bulk carbon nanotubes compacted by spark plasma sintering. Mater Sci Eng A. 2013;573:12–7.
[22] Gui X, Cao A, Wei J, Li H, Jia Y, Li Z, et al. Soft, highly conductive nanotube sponges and composites with controlled compressibility. ACS Nano. 2010;4(4):2320–6.
[23] Gui X, Wei J, Wang K, Cao A, Zhu H, Jia Y, et al. Carbon nanotube sponges. Adv Mater. 2010;22(5):617–21.
[24] Volkov AN, Zhigilei LV. Heat conduction in carbon nanotube materials: Strong effect of intrinsic thermal conductivity of carbon nanotubes. Appl Phys Lett. 2012;101:4.
[25] Volkov AN, Zhigilei LV. Scaling laws and mesoscopic modeling of thermal conductivity in carbon nanotube materials. Phys Rev Lett. 2010;104(21):3–6.
[26] Chalopin Y, Volz S, Mingo N. Erratum: Upper bound to the thermal conductivity of carbon nanotube pellets (Journal of Applied Physics (2009) 105 (084301)). J Appl Phys. 2010;108(3):2009–10.
[27] Yang X, Chen D, Han Z, Ma X, To AC. Effects of welding on thermal conductivity of randomly oriented carbon nanotube networks. Int J Heat Mass Transf. 2014;70:803–10.

[28] Zhang H, Li J, Yao K, Chen L. Spark plasma sintering and thermal conductivity of carbon nanotube bulk materials. J Appl Phys. 2005;97(11):11–6.
[29] Li J, Wang L, He T, Jiang W. Transport properties of hot-pressed bulk carbon nanotubes compacted by spark plasma sintering. Carbon N Y. 2009;47(4):1135–40.
[30] Zhang H, Li J, Zhang B, Yao K, Liu W, Wang H. Electrical and thermal properties of carbon nanotube bulk materials: Experimental studies for the 328–958 K temperature range. Phys Rev B. 2007;75(20):1–9.
[31] Ma W, Liu Y, Yan S, Miao T, Shi S, Xu Z, et al. Chemically doped macroscopic graphene fibers with significantly enhanced thermoelectric properties. Nano Res. 2018;11(2):741–50.
[32] Vavro J, Llaguno MC, Fischer JE, Ramesh S, Saini RK, Ericson LM, et al. Thermoelectric power of p-doped single-wall carbon nanotubes and the role of phonon drag. Phys Rev Lett. 2003;90(6):4.
[33] Shimizu S, Shiogai J, Takemori N, Sakai S, Ikeda H, Arita R, et al. Giant thermoelectric power factor in ultrathin FeSe superconductor. Nat Commun. 2019;10(1):1–7.
[34] Zhao W, Liu Z, Sun Z, Zhang Q, Wei P, Mu X, et al. Super paramagnetic enhancement of thermoelectric performance. Nature. 2017;549(7671):247–51.
[35] Shautsova V, Sidiropoulos T, Xiao X, Güsken NA, Black NCG, Gilbertson AM, et al. Plasmon induced thermoelectric effect in graphene. Nat Commun. 2018;9(1):1–9.
[36] Barnard AW, Zhang M, Wiederhecker GS, Lipson M, McEuen PL. Real-time vibrations of a carbon nanotube. Nature. 2019;566(7742):89–93.
[37] Elyamny S, Dimaggio E, Magagna S, Narducci D. High power thermoelectric generator based on vertical silicon nanowires. Nano Lett. 2020;20(7):4748–53.
[38] Tanaka H, Kanahashi K, Takekoshi N, Mada H, Mada H, Takenobu T. Thermoelectric properties of a semicrystalline polymer doped beyond the insulator-to-metal transition by electrolyte gating. Sci Adv. 2020;6(7):1–9.
[39] Noh J, Tan J, Yadav DR, Wu P, Wu P, Xie KY, et al. Understanding of lithium insertion into 3d porous carbon scaffolds with hybridized lithiophobic and lithiophilic surfaces by in-operando study. Nano Lett. 2020;20(5):3681–7.
[40] Hu P, Lyu J, Fu C, Gong W, Lu W, Liao J, et al. Multi-functional aramid nanofiber/carbon nanotube hybrid aerogel films. ACS Nano. 2020;14(1):688–97.
[41] Ichinose Y, Yoshida A, Horiuchi K, Fukuhara K, Komatsu N, Gao W, et al. Solving the thermoelectric trade-off problem with metallic carbon nanotubes. Nano Lett. 2019;19(10):7370–6.
[42] Dasbach M, Pyschik M, Lehmann V, Parey K, Rhinow D, Reinhardt HM, et al. Assembling carbon nanotube architectures. ACS Nano. 2020;14(7):8181–90.
[43] Selim MM, El-Safty SA. Vibrational analysis of an irregular single-walled carbon nanotube incorporating initial stress effects. Nanotechnol Rev. 2020;9(1):1481–90.
[44] Jiang Q, Zhang Q, Wu X, Wu L. Interfacial characteristics of a carbon nanotube-polyimide nanocomposite by molecular dynamics simulation. Nanotechnol Rev. 2020;9(1):136–45.
[45] Liu J, van der Zee B, Alessandri R, Sami S, Dong J, Nugraha ML, et al. N-type organic thermoelectrics: demonstration of $ZT >$ 0.3. Nat Commun. 2020;11(1):1–9.
[46] Wang X, Suwardi A, Lim SL, Wei F, Wu J. Transparent flexible thin-film p–n junction thermoelectric module. NPJ Flex Electron. 2020;4(1):1–9.
[47] Zaumseil J, Statz M. Charge and thermoelectric transport in polymer-sorted semiconducting single-walled carbon nanotube networks. Nano Lett. 2020;14:11.
[48] Zhang D, Zhang Y, Miao M. Metallic conductivity transition of carbon nanotube yarns coated with silver particles. Nanotechnology. 2014;25(27):275702.
[49] Duan Q, Wang S, Wang Q, Li T, Chen S, Miao M, et al. Simultaneous improvement on strength, modulus, and elongation of carbon nanotube films functionalized by hyperbranched polymers. ACS Appl Mater Interfaces. 2019;11(39):36278–85.